Published in final edited form as:
Curr Med Chem. 2011 ; 18(14): 2103–2114.

Magnetomotive Molecular Nanoprobes

Renu John[1] and **Stephen A. Boppart**[*,1,2]

[1]Beckman Institute for Advanced Science and Technology, University of Illinois at Urbana-Champaign, 405 North Mathews Avenue, Urbana, IL, 61801, USA

[2]Departments of Electrical and Computer Engineering, Bioengineering, and Medicine, University of Illinois at Urbana-Champaign, 405 North Mathews Avenue, Urbana, IL, 61801, USA

Abstract

Tremendous developments in the field of biomedical imaging in the past two decades have resulted in the transformation of anatomical imaging to molecular-specific imaging. The main approaches towards imaging at a molecular level are the development of high resolution imaging modalities with high penetration depths and increased sensitivity, and the development of molecular probes with high specificity. The development of novel molecular contrast agents and their success in molecular optical imaging modalities have lead to the emergence of molecular optical imaging as a more versatile and capable technique for providing morphological, spatial, and functional information at the molecular level with high sensitivity and precision, compared to other imaging modalities. In this review, we discuss a new class of dynamic contrast agents called magnetomotive molecular nanoprobes for molecular-specific imaging. Magnetomotive agents are superparamagnetic nanoparticles, typically iron-oxide, that are physically displaced by the application of a small modulating external magnetic field. Dynamic phase-sensitive position measurements are performed using any high resolution imaging modality, including optical coherence tomography (OCT), ultrasonography, or magnetic resonance imaging (MRI). The dynamics of the magnetomotive agents can be used to extract the biomechanical tissue properties in which the nanoparticles are bound, and the agents can be used to deliver therapy *via* magnetomotive displacements to modulate or disrupt cell function, or hyperthermia to kill cells. These agents can be targeted *via* conjugation to antibodies, and *in vivo* targeted imaging has been shown in a carcinogen-induced rat mammary tumor model. The iron-oxide nanoparticles also exhibit negative T2 contrast in MRI, and modulations can produce ultrasound imaging contrast for multimodal imaging applications.

Keywords

Magnetomotion; molecular imaging; optical coherence tomography; hyperthermia; superparamagnetic iron oxide nanoparticles; targeting

1. INTRODUCTION

Molecular imaging in living organisms including humans is aimed at the visualization, characterization and measurement of biological processes at a cellular level or molecular level using *in vivo* methods. Spectacular advances in therapeutics field of biomedical

[*]Address correspondence to this author at the Beckman Institute for Advanced Science and Technology, Departments of Electrical and Computer Engineering, Bioengineering, and Medicine, University of Illinois at Urbana-Champaign, 405 North Mathews Avenue, Urbana, IL, 61801, USA; Tel: 217-333-8598; Fax: 217-333-5833; boppart@illinois.edu.

imaging in the past two decades have resulted in the transformation of anatomical imaging to molecular-specific imaging. The developments in chemistry, nanotechnology, biotechnology, and engineering have had a profound impact on the biomedical imaging research community, allowing scientists to identify, follow, and quantify subcellular biological processes and pathways within a living organism. The recent developments in nano-sized particles and devices that can be conjugated with several functional molecules including tumor-specific ligands, antibodies, anticancer drugs, and fluorescent imaging probes have revolutionized the arena of cancer therapeutics and diagnostic imaging. Knowing the relationship between the occurrence of various molecular targets to diseases like cancer, and the deliverable concentrations of targeted agents, monitoring these targets through molecular imaging would play an important role in oncology, for example, by aiding the early detection of malignancies, locating metastatic disease, staging tumors, evaluating the availability of therapeutic targets, and monitoring the efficacy of treatment.

The goal of biomedical imaging is to provide structural and functional information, and to visualize biological processes *in vivo*, from the nanoscale to the molecular, cellular, and systems scale, noninvasively. Development of high resolution imaging modalities with high penetration depths and increased sensitivity has been one major stream of research towards imaging at a molecular level. The current field of biomedical imaging comprises a multitude of tools like magnetic resonance imaging (MRI), x-ray computed tomography (CT), ultrasonography (US), positron emission tomography (PET), and single photon emission computed tomography (SPECT) that have developed over the last century, while optical technologies including optical coherence tomography (OCT) and microscopy, multiphoton microscopy (MPM), and diffusion optical tomography are emerging as promising modalities for optical molecular imaging. The sensitivity and specificity of imaging and detection for these imaging modalities can be enhanced by the introduction of a molecular probe, although ongoing research efforts have also been directed at sensing intrinsic optical molecular signatures.

The optical imaging modalities have unique capabilities to distinguish cells and tissues based on their optical scattering and absorption properties. Most of the optical imaging techniques rely on the absorption and scattering changes of light as it traverses biological tissue, providing optical signal changes that carry information about the tissues. Biological samples are fairly transparent in the near-infrared (NIR) window of the electromagnetic spectrum [650-1350 nm], which is often termed as the biological window, making this spectral region ideal for optical imaging applications. The contrast generated could be either from the endogenous signals from specific molecules or from targeted agents attached to specific molecules. The development of novel molecular contrast agents and their success in molecular optical imaging modalities have led to the emergence of molecular optical imaging as a more versatile and capable technique for providing morphological, spatial, and functional information at the molecular level with high sensitivity and precision, compared to other imaging modalities. This review article will provide a brief overview of the development of a new class of dynamic contrast agents called magnetomotive molecular nanoprobes, will discuss their *in vivo* applications in optical molecular imaging, and will address the challenges and future directions on how to improve the state-of-theart cancer diagnostics and therapy using these novel contrast agents and mechanisms.

2. MOLECULAR NANOPROBES

The recent developments in nanotechnology have contributed enormously to the field of nanomedicine, resulting in a wide variety of novel agents with sizes ranging from 5-200 nanometers for applications in bioimaging, biosensing and therapy. A wide variety of nanostructures including nanoparticles [1-4], nanospheres [5,6], nanoshells [7-13], nanorods

[14-20], nanocages [20-23], nanotubes [23-27], nanostars [28], nanowires [29, 30] and quantum dots [31-35] have been fabricated using materials that are optically or chemically active. Each exhibit some optical property that can be exploited by existing imaging modalities to achieve additional contrast information. Nanoparticles made of materials like gold, silver, iron oxide, gadolinium, carbon, and a wide variety of polymers, have been used as optical contrast agents with different optical imaging modalities. In addition to their primary aim of generating molecular-specific contrast, these nanoparticle agents can be functionalized to target specific sites, enabling applications such as site-specific delivery of drugs [36-41], nucleotides, proteins or genetic materials, and hyperthermia [40, 42, 43].

A number of factors determine the clinical usefulness of nanoparticles. Their physical and functional biokinetic properties, clearance profiles, biodistribution, biocompatibility, and long-term toxicity need to be carefully considered for their potential use in *in vivo* applications. Nanoparticles having sizes smaller than 50 nm show prolonged blood half-life times compared to larger ones. Larger particles are quickly uptaken by phagocytic cells. Expectedly, particles with longer circulation times have a greater probability of reaching the target sites. Hydrophilic particles have a longer blood half-life compared to hydrophobic particles. Particles that are hydrophilic in nature with no charge on them, or have very low negative charges, are known to have longer blood half-life times. Generally, nanoparticles used for biomedical applications are coated with different surfactants and agents to prevent agglomeration, improve their dispersibility and biocompatibility in physiological media, reduce toxicity, and alter pharmacokinetics and biodistribution [36]. The conjugation with various functional groups and targeting ligands also is aided by choosing a desirable surface coating.

2.1. Superparamagnetic Iron Oxide Magnetic Nanoparticles (SPIONs)

The use of iron oxide for *in vitro* diagnostic applications has been in practice for over 40 years [44]. Superparamagnetic iron oxide magnetic nanoparticles (SPIONs) have a very promising role as ultra-sensitive molecular-specific imaging nanoprobes. Magnetitie (Fe_3O_4), which is a common form of iron oxide, has preferred qualities such as high magnetization values, high specific heat absorption rates (for hyperthermia), and well-known biocompatibility for *in vivo* applications. Iron oxide nanoparticles, due to their small sizes and extremely large relative surface area, exhibit superparamagnetic phenomena and find numerous applications in the field of biomedical imaging. Their unique paramagnetic properties with strong T2 and negative T2* contrast have made them attractive contrast agents in MRI [45].

SPIONs can be synthesized through different methods, the simplest one being a coprecipitation method where a mixture of ferrous and ferric ion salts in alkaline medium and an oxygen-free environment yield iron oxide nanoparticles of sizes from 20 to 90 nm [36, 46-49]. The coprecipitation is usually carried out in the presence of materials like dextran and other polyols that form an outer coating over the nanoparticles. The size of particles depends on the ratio of the ions, types of salts, pH, and ionic strengths of the solutions. The main drawback of this technique, however, is the lack of precise control over nanoparticle size. Other techniques like microemulsion techniques [50, 51] and thermal decomposition methods [52] provide better control over the size distributions of the synthesized particles. Different methods of preparation of iron oxide nanoparticles including variations of the above coprecipitation technique have been discussed in detail by Gupta and Gupta [47]. Both inorganic metal and metal oxides, and organic polymers and monomers, have been used to coat iron oxide nanoparticles. Iron oxide nanoparticles coated with materials like dextran, or dextran derivatives [53, 54], albumin [54], polyethylene glycols (PEGs) [45, 55], and polyvinylpyrrolidone [56], have been reported to have high biocompatibility for *in vivo* applications. Numerous works have been reported over the past

two decades on functionalizing iron oxide nanoparticles with a number of targeting agents like proteins [36, 57, 58], antibodies [46, 59-61], polypeptides [40, 62, 63], and oligonucleotides [64, 65]. The ease of their fabrication with tailored surface chemistry, biocompatibility, and bioconjugation possibilities have made them attractive choices for use in different imaging modalities and biomedical applications.

2.2. Targeted Magnetic Nanoprobes

SPIONs can be localized primarily through two mechanisms, active and passive targeting. The traditional approach for nanoparticle-based therapy is aimed at the passive targeting of nanoparticles to specific sites such as in tumors by exploiting the enhanced permeability and retention (EPR) effect associated with the leaky vasculature [66], thereby allowing nanoparticles to readily extravasate and accumulate in the tumors. The lack of lymphatic drainage in these inflamed tissues also aids accumulation of nanoagents. This would enable imaging of these malignant sites and delivery of therapeutic drugs. However, experiments have shown that nanoparticles most likely undergo opsonization in blood, resulting in their fast uptake by the reticulo-endothelial system (RES), and their final clearance from the circulation. Intravenous injections of SPIONs have been shown to accumulate mostly in the RES of the liver and spleen. As a result, a relatively low concentration of nanoparticles at targeting sites has become a major obstacle in using them for tumor imaging or therapy. Surface modifications, such as coating nanoparticles with polymers like PEG-THIOL, have proven useful to protect the nanoparticles from being captured by the RES, thus increasing their blood half-lives.

Active targeting of SPIONs with target-specific ligands is another way to promote selective binding to biomarkers for target-specific accumulation. Knowledge of expression profiles of various biomarkers in different pathological conditions will allow the physician to identify abnormalities at an earlier stage, monitor disease progression, and efficacy of treatment. The ability to functionalize the surface of these nanoprobes allows cell or tissue-specific targeting. Along with the synthesis of these nanoprobes, the chemistry of bioconjugation has also contributed significantly to the development of targeted probes that can be conjugated to different biomarkers, proteins, peptides, or oligonucleotides. Development of functionalized nanoprobes for *in vivo* targeting is extremely challenging and involves multidisciplinary skills. Efficient ways to direct these nanoparticles to organs, tissues, tumors, and malignant cells have been reported by conjugating the nanoparticles with enzymes, proteins, antibodies, nucleotides, or peptide ligands. Various biomarkers and oncoproteins like *HER2* [46, 60, 61, 67, 68], or MMPs [69-71] that are known to be over-expressed at the sites of malignancy have been targeted using different conjugation techniques. The conjugating procedures depend on the nature of the nanoparticle coating and the conjugating ligand or proteins. Targeted molecular imaging using functionalized nanoprobes targeted to the *HER2* antigen has been demonstrated on two cell lines with different *HER2* expression levels [72] (Fig. **1**). The Fc-directed conjugation of antibodies to iron oxide magnetic nanoparticles (MNPs) aids their efficient immunospecific targeting through the free Fab portions. Multifunctionality is one of the most desirable qualities of these targeted nanoprobes, giving rise to diagnostic and therapeutic agents that can simultaneously act as contrast agents in imaging as well as therapeutic and drug delivery agents, aiding the treatment, and monitoring the progress.

Magnetic nanoparticles that act as MR contrast agents can provide information on the location of the probe, and can also be tailored as NIR fluorescent (NIRF) imaging probes by conjugating cleavable Cy5.5-derivatized peptides to their surface [73]. Contrast enhancement by MR results from a core of superparamagnetic iron oxide, while the NIRF signal results from amino-CLIO. A magnetic nanoparticle with a surface of aminated, cross-linked dextran has been used to attach a variety of biological molecules, including the tat

peptide of the HIV tat protein, transferrin, and oligonucleotides, and provides a convenient platform for the attachment of Cy5.5 peptides. SPIONs tagged with transfection agents have been reported as intracellular contrast agent for nuclear MRI cell tracking *in vivo* [74]. Intracellular SPIO colloid uptake in live cells has been quantified using cell magnetophoresis.

2.3. Microsphere Encapsulations of Magnetic Nanoparticles

SPIONs can be encapsulated into protein-shelled microspheres with sizes up to a few microns for applications involving imaging, targeted drug delivery, and therapy. These microspheres, due to their relatively large size, remain in the vasculature after intravenous administration, and are suitable for identifying regions of altered perfusion (leaky or ruptured vessels), and for targeting to specific markers that are over-expressed in regions of angiogenesis (in cancer) and atherosclerosis (in heart disease), to provide some examples. Protein microspheres consisting of a hydrophobic core composed of vegetable oil and a hydrophilic protein shell with sizes from 2- 5 microns have been reported as scattering contrast agents in OCT [75-79] (Fig. **2**). These microspheres have been encapsulated with lipids, NIR dyes, and various nanoparticles including gold, carbon, melanin, and superparamagnetic iron oxide nanoparticles in their core and shell to effectively work as multimodal contrast agents in NIRF imaging, ultrasound, MRI, OCT, and MM-OCT [76-78]. Owing to the presence of iron oxide nanoparticles in their core, these microspheres can be dynamically modulated using an external magnetic field, thereby creating dynamic contrast in biological samples and additionally serving as dynamic probes that are discussed in the next section.

Protein microspheres have been targeted to alpha (v) beta (3) integrin receptors by conjugating an RGD peptide sequence to the outer surface of these microspheres [76-77]. These integrin receptors play an important role in the development of cancer or angiogenesis and are also over-expressed at sites of atherosclerosis. RGD-functionalized microspheres have been successfully tested on cell lines that overexpress these integrin receptors [76, 77]. The possibility of controlling the *in vivo* rupture of microspheres to release its shell or core contents is another promising application of these agents as a means for drug administration and delivery of genetic material and proteins. These targeted protein microspheres would therefore serve as potential site-specific drug delivery vehicles with the capacity for relatively high payloads.

3. APPLICATIONS

3.1. Magnetomotion

A wide variety of molecular specific contrast agents have been studied for coherence imaging applications. All previous scattering-based probes have relied of their static scattering nature for the enhancement of the optical signal or to provide contrast in imaging. One of the main drawbacks of scattering-based probes is the inherent background noise that arises from the static background scattering of the tissues. Hence, the endogenous scattering from the tissue structures can be separated from the scattering caused by the contrast agents only through prior information about the tissue structure, i.e. by comparing the images before and after the administration of the contrast agents. Dynamic probes that can be modulated externally offer an elegant solution to this problem. Small perturbations in scattering can be created using dynamic modulation of the probes and the unperturbed background signal can be filtered out efficiently through post-acquisition data processing. Coherent imaging modalities offer high resolution and sensitivity at nanoscales, enabling functional imaging at the subcellular level, such as tracking biological processes, detecting

flow, and sensing dynamic modulations and displacements at a nanoscale. In addition, the heterodyne detection capabilities can produce images with exceptionally high SNR.

Magnetomotion refers to the dynamic modulation of magnetic agents on application of an external magnetic field. Magnetomotion, in general, can be rotation or translation. A particle with a permanent magnetic moment (strong effect) or with a highly anisotropic shape (weak effect) can be aligned with an applied magnetic field through a rotational motion [80]. Different properties like optical scattering cross-section, polarization-dependent scattering, or birefringence can be modulated through this change in alignment due to rotation, and hence, any imaging modality such as OCT or PS-OCT could exploit this modulation to create magnetomotive contrast while imaging. An example of related work is the determination of antibody binding using birefringence measurements on alignment of magnetic nanoparticles [81]. Also, magnetic contrast agents whose fluorescence is modulated by rotation have been developed for microscopy [82]. In another work, a dynamic mode of optical contrast termed as gyromagnetic imaging [28] has been reported recently using gold nanostars with superparamagnetic cores. Gold nanostars with superparamagnetic cores are driven by a rotating magnetic field gradient to produce periodic variations in NIR scattering intensities detected in a dark-field microscope set-up. This periodic “twinkling” in response to a rotating magnetic field gradient results in a frequency-modulated signal that is converted into Fourier-domain images with a dramatic reduction in background.

Magnetomotion of contrast agents through an externally modulating magnetic field is an excellent mechanism for achieving dynamic contrast. This can be realized by using paramagnetic particles as contrast agents. Human tissue exhibits an extremely weak magnetic susceptibility ($\chi<|10^{-5}|$). Hence the employment of magnetic probes with $\chi\sim1$ provides a large potential dynamic range of magnetic contrast. Iron oxide, such as magnetite, with paramagnetic properties and $\chi\sim1$ is a good candidate with known biocompatibility after coating with polymers such as dextran. Paramagnetic iron oxide MNPs have been already approved as contrast agents in MRI. These micron and nano-sized MNPs can be actuated externally using a modulating magnetic field. In the presence of a high magnetic field gradient, particles with high magnetic susceptibility embedded in tissue experience a gradient force, and ferromagnetic particles rotate to align their internal magnetization along the field. The resulting magnetomotion of the MNPs and the perturbation of the surrounding cells and extracellular matrix result in a change in the scattering properties of the local tissue microenvironment under observation (Fig. **3a**). In an elastic medium, the particle returns to its original position and orientation after removal of the magnetic field. This permits modulation of its position by repetitively modulating the magnetic field. The resulting increase in contrast due to magnetomotion can be effectively detected by a coherent interferometric imaging technique like OCT.

3.2. Magnetomotive Optical Coherence Tomography (MMOCT)

The ability to capture both the amplitude and phase of a coherent signal using interferometric techniques [83-91] has enabled the retrieval of additional valuable information from the sample. The magnetomotive response of the tissue phantom to different magnetic field excitations can easily be demonstrated by performing M-mode imaging at one point on a tissue phantom. A step excitation or a sweep of frequencies applied to the sample under study is used to extract information about the mechanical and viscoelastic properties of the biological tissue. Doing this, one can find the resonant mechanical frequency of the biological sample as well.

A standard OCT system can be readily modified to enable MMOCT imaging [79]. In the MM-OCT system, the magnetic field is applied using a solenoid, and imaging is performed

on the sample immediately below the solenoid bore. Within the imaging volume of the sample, the radial components of the magnetic field are negligible and the magnetic field gradient is predominantly in the axial direction. The MNPs under the effect of magnetomotion due to an axial magnetic field result in a change in amplitude and phase of the interference pattern in a spectral domain OCT system. A sinusoidal magnetic field excitation with a frequency close to the mechanical resonance of the biological sample is used to perform MM-OCT imaging.

Magnetomotive contrast has been demonstrated first with OCT by Oldenburg *et al.* [92] with a 3-D scaffold of macrophage cells loaded with iron oxide microparticles. The scatterers themselves do not exhibit significant optical scattering, but act as transducers, displacing the adjacent scatterers such as cells and organelles, and hence, can be detected using this contrast mechanism (Fig. **3b-d**). Iron oxide MNPs have been topically administered to highly scattering media such as chicken skin (Fig. **4**) and the sensitivity of this technique has been demonstrated *in vitro* [93]. This ability to track magnetically-labeled cells on micron-scales in scattering tissue scaffolds as well as in *in vitro* environments provides a new investigation tool to study the *in vivo* dynamics and subcellular transport phenomena. *In vivo* MM-OCT imaging of MNPs in the digestive tract of an African frog tadpole was demonstrated [79]. Rejection of physiological motion for *in vivo* imaging was accomplished by acquiring two successive axial scans with the magnetic field off and a third with the field on, and comparing the signal changes between the on and off scans (magnetomotion) with those between the two off scans (physiological motion). The main drawback of this study was the long imaging times needed to take three B-mode images for each measurement. This is not feasible for *in vivo* and real-time applications. Also, this method only tracked the amplitude of the OCT interference signal.

The use of optical phase to obtain sub-wavelength displacement sensitivity is very powerful for imaging biological samples [94]. A differential-phase OCT system was proposed to detect (but not image) the magnetomotion of MNP-laden macrophages in an animal model [95]. A MM-OCT algorithm has been proposed that measures modulation in the optical phase due to magnetomotion and thereby deduce the sample displacement [96]. Magnetomotive signals from a specimen under study can be isolated with the help of two B-mode MM-OCT images, one image with the field off and one with the modulating field on. We can couple the mechanical excitation with the B-mode OCT scanning by modulating the magnetic field several cycles during the time taken to mechanically scan the imaging beam. Transverse Fourier spectra of B-mode images with and without the magnetic field indicate the contribution from magnetomotion compared to the structural contribution (Fig. **5**). This system is capable of detecting MNP concentrations as low as ~2 nM within the sample, and from the phase information obtained through interferometric detection, displacements of MNPs as low as a few tens of nanometers can be measured.

The dynamic behavior and transport of magnetic nanoprobes in biological tissues for different concentrations and temperatures can be effectively tracked using the MM-OCT technique [97]. *Ex vivo* magnetomotive imaging of diffusing MNPs in several types of tissues has been demonstrated. Using this method, it is possible to quantitatively estimate the diffusion and transport of MNPs in tissues and viscoelastic materials (Fig. **6**). The studies have shown that the transport of MNPs in tissues depends on the temperature and the elastic nature of the tissue or supporting media. These results show that the magnetomotive technique would aid in understanding the actual localization and accumulation of functionalized MNPs targeted to specific sites. *In vivo* imaging of dynamic functionalized iron oxide MNPs has been demonstrated using MM-OCT in a pre-clinical mammary tumor model [98]. These MNPs are antibody functionalized to target the human epidermal growth factor receptor 2 (*HER2 neu)* protein, which is overexpressed in about 30% of human

invasive breast carcinomas [72, 99]. Using targeted MNPs, *in vivo* MM-OCT images exhibit strong magnetomotive signals in mammary tumor, and no significant signals were measured from tumors of rats injected with nontargeted MNPs or saline (Fig. **7**). This study has also demonstrated the feasibility of multimodal imaging using MNPs as dynamic contrast agents for *in vivo* tumor imaging using MM-OCT and MRI. These magnetic nanoprobes can also be incorporated into systems that require magnetic manipulation of nanoprobes, including magnetic field-guided drug delivery systems for cancer treatment.

The MNPs that are embedded in tissues or elastic materials act as dynamic nanotransducers that can be actuated externally using a magnetic field to evaluate the viscoelastic properties of the medium in which they are dispersed. The scatterers undergo underdamped oscillations when the magnetic field is applied step-wise (Fig. **8**) [100], allowing for the measurement of the natural frequencies of oscillation of the samples. The sample embedded with MNPs and modulated with a sweep of frequencies exhibit mechanical resonance modes [101], which are well described by a linear damped harmonic oscillator model. This resonant frequency is the natural frequency of oscillation of each particular type of tissue and varies strongly with the elastic modulus of the sample. Direct correlation has been observed between the elastic modulus of biological tissues and their experimentally-measured mechanical resonant frequencies [97]. Hence, this technique can be used to extract the mechanical vibration spectra and therefore the elastic properties of biological tissues. This new method of magnetomotive optical coherence elastography (MM-OCE) would also find applications in real-time non-destructive analysis of soft viscoelastic tissues and various polymers.

In another interesting application, Kim *et al.* [102] have applied the principle of magnetomotion to optical Doppler tomography to enhance the contrast of flowing red blood cells. In a system of flowing SPIONs, the contrast due to the subsurface-scatterer flow, and hence the Doppler shifts, can be enhanced by activating mechanical motion in the nanoparticles. Magnetomotive optical Doppler tomography (MM-ODT) has been demonstrated on Doppler images of flowing SPIONs under the influence of an externally applied magnetic field gradient [103].

Laser speckle imaging (LSI) is another imaging technique where magnetomotion may be exploited for achieving better image contrast. This technique may be useful in wide-field imaging applications for the detection of suspicious malignancies in biological tissues and defects. In magnetomotive (MM-) LSI, a magnetic field modulation of SPIONs embedded in the sample specimen could change the speckle properties of the collected images. Speckle spatial frequency analysis [104] or speckle variance properties [105, 106] of interframe intensity variance of OCT structural images acquired consecutively in a time dependent manner could be analyzed for detecting the flow or motion of sample features on micron scales. These techniques would find applications in imaging the microvasculature and blood flow. Kim *et al.* [107] have shown that magnetic activation of SPIONs with an externally-applied, high-strength magnetic field gradient modulates the speckle flow index (SFI) values estimated from speckle contrast analysis of collected images. Subsequently, the contrast in laser speckle images has been enhanced by the magnetomotion of the nanoparticles.

3.3. Magnetomotive Ultrasound

SPIONs can act as dynamic contrast agents in ultrasonography using external time varying magnetic fields. In magnetomotive ultrasound (MM-US) imaging, circulating MNPs are subjected to modulating magnetic fields and these modulations are detected as frequency shifts in Doppler ultrasound measurements [108, 109]. Detection of magnetomotive modulations in *ex vivo* liver tissue has been demonstrated through ultrasonography. Liver specimens were collected from rats pre-injected with MNPs. The MNPs accumulated in the macrophages in liver. Doppler ultrasound measurements could detect the frequency shifts

corresponding to the micron-scale displacements of iron-laden macrophage cells under a time-varying magnetic field modulation. These results indicate the potential of MM-US for molecularly-sensitive imaging on a cellular scale using ultrasound.

Magnetic nanoparticles also provide a new possibility to increase contrast by magnetomotive manipulation during photoacoustic imaging. A multi-functional imaging system integrating ultrasound and photoacoustic imaging with magnetic manipulation can take advantage of each single modality by providing anatomical images and molecular function with greater contrast. A new class of gold nanoshells with a superparamagnetic iron oxide core (SPIO–Au nanoshells) has been shown to have desirable optical and magnetic properties, enabling multimodal imaging [110, 111]. These nanoparticles can be guided to a specific site using an external guiding magnetic field, thereby enhancing the efficacy of nanoshell-mediated photothermal therapy. With a significant absorbance in the NIR region of the electromagnetic spectrum, they would efficiently act as photothermal agents for therapy. They would also find applications as dynamic contrast agents for *in vivo* real-time MM-OCT and MRI.

3.4. Magnetic Hyperthermia

Iron oxide magnetic nanoparticles have shown to act as ideal agents for hyperthermia effects where alternating electromagnetic fields can be used to heat the nanoparticles, thereby directing thermal damage to passively- or actively-targeted cells and tissues. In magnetic hyperthermia, the energy in the magnetic field is transformed to heat through different mechanisms like eddy current loss, hysteresis loss, and relaxation loss due to Neel relaxation and Brownian relaxation. Larger particles (size ~ >30 nm) are generally regarded as having multiple domains and the main mechanism of heat generation is through hysteresis losses, while smaller particles (single domain particles) generate heat by Neel–Brownian relaxations [112, 113]. The transition between the two mechanisms occurs between 5-12 nm for various materials and is also frequency dependent.

Magnetic hyperthermia can potentially reduce the adverse side effects caused to normal tissue through traditional treatment methods like systemic chemotherapy and radiation therapy. Also, magnetic hyperthermia effects can make the tumor tissue more susceptible or sensitized to radiation and other therapies [114]. It has been shown that magnetic hyperthermia can raise the temperature of localized regions in the body to temperatures in the range of 42-55° C [115-120] without any systemic effects. Magnetic nanoparticle suspensions that are biocompatible can be heated using alternating electromagnetic fields. The rise in temperature depends upon the size, shape, and magnetic properties (permeability, losses and saturation moment) of the material, and the amplitude and frequency of the applied magnetic field. The magnitude of the magnetic field to which a human body can be exposed, however, is limited. The product of applied field strength (H) and frequency (*f*) should be limited to 6×10^6 Oe-Hz to prevent injury due to excessive direct tissue heating. Ferrofliuds that are suspensions of iron oxide nanoparticles are ideal for this type of applications for their high biocompatibility and low toxicities while having high specific absorption rates. Hilger *et al.* [121] have shown that magnetic hyperthermia can induce cell apoptosis in cancerous cells by heating in the range of 41-46 °C. Heating over 46 °C can also result in thermoablation, leading to necrotic death of cancerous tissue.

It has also been found that the magnetic properties desirable for hyperthermia applications of iron oxide nanoparticles can be improved by substituting Fe with other metals like Mn, Co, Al, or Zn, and hence the amount of nanoparticles that may be needed for inducing hyperthermia could be lowered. A number of other nanoparticles have been reported as being capable of providing magnetomotive contrast in imaging and suitable for hyperthermia applications like gold nanostars with an iron oxide core. Gd-doped iron oxide

nanoparticles were reported for use in tumor therapy *via* magnetic hyperthermia in *in vivo* mouse models [122].

4. CONCLUSIONS AND FUTURE PERSPECTIVES

Magnetomotive molecular probes are promising tools for the noninvasive *in vivo* visualization of pathological conditions at the sub-cellular and cellular level. These probes have also demonstrated their capabilities as therapeutic tools for targeted drug delivery and hyperthermia applications. Molecular specificity remains the key strength of this technology that attracts the use of various probes in virtually all imaging modalities. In addition, these probes can be flexibly engineered and fabricated. Being multimodal and multifunctional, they have been used in many of the current clinical imaging modalities such as MRI, ultrasound, x-ray computed tomography, and nuclear imaging (PET and SPECT).

The evolution of these molecular imaging probes continues to advance, with high optimism among the research communities as a hot topic of research in the coming years. Early studies on the synthesis, bioconjugation, targeting to biomarkers, *in vitro* evaluations, and pre-clinical investigations using small animal models have been promising and successful. Recent research in this field has primarily been focused on the development of molecular imaging agents and tools. Future research investigations are now being directed at the translation of these technologies to clinical applications, having nanoparticle-based diagnostic imaging agents and modalities enter clinical trials. In parallel, there is continued research in chemistry and biology, seeking new targeting moieties. Research in probe pharmacokinetics and modelling together with experimental small-animal multimodal imaging systems are being utilized to understand their biodistribution and dynamics in biological systems. Given the prevalence and impact of cancer on our lives, cancer detection, imaging, and therapy are expected to be the earliest applications for these magnetomotive molecular-specific probes.

Optical molecular imaging to date has been successful in catering to the requirements of the biological research community by providing better resolution, specificity, and sensitivity. Optical coherence imaging and microscopy are likely to play a significant role in the detection, diagnosis and evaluation of various cancers, offering real-time tracking and visualization across a range of size scales. New advances in catheter- and endoscope-based OCT technologies allow for the use of magnetomotive probes at internal sites accessed *via* minimally-invasive procedures. With the development of catheters and multimodal imaging tools, magnetomotive OCT has a strong potential to translate to the clinic. These same probes can also find utility in image-guided procedures, contributing to their multimodal multifunctional use. With recent demonstrations of magnetomotive ultrasonography, magnetomotive molecular probes are being explored by other imaging modalities in research like fluorescence and multiphoton imaging, photoacoustic tomography, MRI, and CT, enabling a potential translation to the clinic as multimodal imaging tools and the next generation of therapeutic strategies. Magnetomotive molecular probe-based multimodal imaging is likely to play a unique role in future clinical imaging and treatment practices.

Acknowledgments

We wish to thank the members of the Biophotonics Imaging Laboratory at the Beckman Institute on the University of Illinois at Urbana-Champaign (UIUC) campus for their dedication and insight in this area of research. We also wish to thank our collaborators for their work in fabricating novel probes including Kenneth Suslick, Department of Chemistry, UIUC, and Alex Wei, Department of Chemistry, Purdue University. Finally, we thank our colleagues whose work is represented here for helping advance this field, and apologize to those whose work was not included due to space and depth of coverage constraints. This research was supported in part by the National Institutes of Health (Roadmap Initiative, NIBIB, R21 EB005321; NIBIB R01 EB009073; NCI RC1 CA147096, to S.A.B.). Additional information can be found at http://biophotonics.illinois.edu.

REFERENCES

1. Sokolov K, Follen M, Aaron J, Pavlova I, Malpica A, Lotan R, Richards-Kortum R. Real-time vital optical imaging of precancer using anti-epidermal growth factor receptor antibodies conjugated to gold nanoparticles. Cancer Res. 2003; 63:1999–2004. [PubMed: 12727808]
2. Wax A, Sokolov K. Molecular imaging and darkfield microspectroscopy of live cells using gold plasmonic nanoparticles. Laser Photonics Rev. 2009; 3:146–158.
3. Chamberland DL, Agarwal A, Kotov N, Fowlkes JB, Carson PL, Wang X. Photoacoustic tomography of joints aided by an Etanerceptconjugated gold nanoparticle contrast agent - an *ex vivo* preliminary rat study. Nanotechnology. 2008; 19:095101. [PubMed: 21817663]
4. Lim YT, Noh YW, Kwon JN, Chung BH. Multifunctional perfluorocarbon nanoemulsions for ^{19}F-based magnetic resonance and near-infrared optical imaging of dendritic cells. Chem. Commun. 2009; 45:6952–6954.
5. Kumar R, Ohulchanskyy TY, Roy I, Gupta SK, Borek C, Thompson ME, Prasad PN. Near-infrared phosphorescent polymeric nanomicelles: Efficient optical probes for tumor imaging and detection. ACS Appl. Mater. Interfaces. 2009; 1:1474–1481. [PubMed: 20355951]
6. Glynos E, Koutsos V, McDicken WN, Moran CM, Pye SD, Ross JA, Sboros V. Nanomechanics of biocompatible hollow thin-shell polymer microspheres. Langmuir. 2009; 25:7514–7522. [PubMed: 19379000]
7. Agrawal A, Pfefer TJ, Huang S, Lin AWH, Lee M-H, Drezek RA, Barton JK, Drezek RA, Pfefer TJ. Quantitative evaluation of optical coherence tomography signal enhancement with gold nanoshells. J. Biomed. Optics. 2006; 11:041121.
8. Hirsch LR, Gobin AM, Lowery AR, Tam F, Drezek RA, Halas NJ, West JL. Metal nanoshells. Ann. Biomed. Eng. 2006; 34:15–22. [PubMed: 16528617]
9. Ji XJ, Shao RP, Elliott AM, Stafford RJ, Esparza-Coss E, Bankson JA, Liang G, Luo ZP, Park K, Markert JT, Li C. Bifunctional gold nanoshells with a superparamagnetic iron oxide-silica core suitable for both MR imaging and photothermal therapy. J. Phys. Chem. C. 2007; 111:6245–6251.
10. Lin AWH, Lewinski NA, West JL, Halas NJ, Drezek RA. Optically tunable nanoparticle contrast agents for early cancer detection: model-based analysis of gold nanoshells. J. Biomed. Opt. 2005; 10:064035. [PubMed: 16409100]
11. Puvanakrishnan P, Park J, Diagaradjane P, Schwartz JA, Coleman CL, Gill-Sharp KL, Sang KL, Payne JD, Krishnan S, Tunnell JW. Near-infrared narrow-band imaging of gold/silica nanoshells in tumors. J. Biomed. Opt. 2009; 14:024044. [PubMed: 19405772]
12. Zaman RT, Diagaradjane P, Wang JC, Schwartz J, Rajaram N, Gill-Sharp KL, Cho SH, Rylander HG, Payne JD, Krishnan S, Tunnell JW. *In vivo* detection of gold nanoshells in tumors using diffuse optical spectroscopy. IEEE J. Select. Top. Quant. Electron. 2007; 13:1715–1720.
13. Loo C, Lowery A, Halas N, West J, Drezek R. Immunotargeted nanoshells for integrated cancer imaging and therapy. Nano Lett. 2005; 5:709–711. [PubMed: 15826113]
14. Oldenburg AL, Hansen MN, Ralston TS, Wei A, Boppart SA. Imaging gold nanorods in excised human breast carcinoma by spectroscopic optical coherence tomography. J. Mater. Chem. 2009; 19:6407–6411. [PubMed: 20107616]
15. Oldenburg AL, Hansen MN, Zweifel DA, Wei A, Boppart SA. Plasmon-resonant gold nanorods as low backscattering albedo contrast agents for optical coherence tomography. Opt. Expr. 2006; 14:6724–6738.
16. Troutman TS, Barton JK, Romanowski M. Optical coherence tomography with plasmon resonant nanorods of gold. Opt. Lett. 2007; 32:1438–1440. [PubMed: 17546147]
17. Jana NR, Gearheart L, Murphy CJ. Wet chemical synthesis of high aspect ratio cylindrical gold nanorods. J. Phys. Chem. B. 2001; 105:4065–4067.
18. Nikoobakht B, El-Sayed MA. Preparation and growth mechanism of gold nanorods (NRs) using seed-mediated growth method. Chem. Mater. 2003; 15:1957–1962.
19. Cepak VM, Martin CR. Preparation and stability of template-synthesized metal nanorod sols in organic solvents. J. Phys. Chem. B. 1998; 102:9985–9990.

20. Cho EC, Kim C, Zhou F, Cobley CM, Song KH, Chen JY, Li ZY, Wang LV, Xia Y. Measuring the optical absorption cross sections of Au-Ag Nanocages and Au Nanorods by photoacoustic imaging. J. Phys. Chem. C. 2009; 113:9023–9028.
21. Cang H, Sun T, Li Z-Y, Chen JY, Wiley BJ, Xia YN, Li X. Gold nanocages as contrast agents for spectroscopic optical coherence tomography. Opt. Lett. 2005; 30:3048–3050. [PubMed: 16315717]
22. Chen J, Saeki F, Wiley BJ, Cang H, Cobb MJ, Li Z, Zhang H, Kimmey MB, Li X, Y. Au L, Xia Y. Gold nanocages: bioconjugation and their potential use as optical imaging contrast agents. Nano Lett. 2005; 5:473–477. [PubMed: 15755097]
23. Skrabalak SE, Chen JY, Sun YG, Lu XM, Au L, Cobley CM, Xia Y. Gold nanocages: synthesis, properties,and applications. Accounts Chem. Res. 2008; 41:1587–1595.
24. Choi JH, Nguyen FT, Barone PW, Heller DA, Moll AE, Patel D, Boppart SA, Strano MS. Multimodal biomedical imaging with asymmetric single-walled carbon nanotube/iron oxide nanoparticle complexes. Nano Lett. 2007; 7:861–867. [PubMed: 17335265]
25. De La Zerda A, Zavaleta C, Keren S, Vaithilingam S, Bodapati S, Liu Z, Levi J, Smith BR, Ma TJ, Oralkan O, Cheng Z, Chen XY, Dai HJ, Khuri-Yakub BT, Gambhir SS. Carbon nanotubes as photoacoustic molecular imaging agents in living mice. Nat. Nanotechnol. 2008; 3:557–562. [PubMed: 18772918]
26. Hong H, Gao T, Cai WB. Molecular imaging with single-walled carbon nanotubes. Nano Today. 2009; 4:252–261. [PubMed: 21754949]
27. Pramanik M, Wang LV, Swierczewska M, Green D, Sitharaman B. Single-walled carbon nanotubes as a multimodal-thermoacoustic and photoacoustic-contrast agent. J. Biomed. Opt. 2009; 14:034018. [PubMed: 19566311]
28. Wei Q, Song H-M, Leonov AP, Hale JA, Oh DM, Ong QK, Ritchie K, Wei A. Gyromagnetic imaging: Dynamic optical contrast using gold nanostars with magnetic cores. J. Am. Chem. Soc. 2009; 131:9728–9734. [PubMed: 19435348]
29. Iijima S. Helical microtubules of graphitic carbon. Nature. 1991; 354:56–58.
30. Patolsky F, Zheng G, Hayden O, Lakadamyali M, Zhuang X, Lieber CM. Electrical detection of single viruses. Proc. Natl. Acad. Sci. USA. 2004; 101:14017–14022. [PubMed: 15365183]
31. Parak WJ, Pellegrino T, Plank C. Labelling of cells with quantum dots. Nanotechnology. 2005; 16:R9–R25. [PubMed: 21727419]
32. Morgan NY, English S, Chen W, Chernomordik V, Russo A, Smith PD, Gandjbakhche A. Real time *in vivo* non-invasive optical imaging using near-infrared fluorescent quantum dots. Acad. Radiol. 2005; 12:313–323. [PubMed: 15766692]
33. Smith AM, Ruan G, Rhyner MN, Nie S. Engineering luminescent quantum dots for *in vivo* molecular and cellular imaging. Ann. Biomed. Eng. 2006; 34:3–14. [PubMed: 16450199]
34. Rhyner MN, Smith AM, Gao X, Mao H, Yang L, Nie S. Quantum dots and multifunctional nanoparticles: new contrast agents for tumor imaging. Nanomedicine. 2006; 1:209–217. [PubMed: 17716110]
35. Mazumder S, Dey R, Mitra MK, Mukherjee S, Das GC. Review: biofunctionalized quantum dots in biology and medicine. J. Nanomater. 2009; 2009:815734.
36. Gupta AK, Wells S. Surface-modified superparamagnetic nanoparticles for drug delivery: Preparation, characterization, and cytotoxicity studies. IEEE Trans. Nanobiosci. 2004; 3:66–73.
37. Sinha R, Kim GJ, Nie S, Shin DM. Nanotechnology in cancer therapeutics: bioconjugated nanoparticles for drug delivery. Mol. Cancer Ther. 2006; 5:1909–1917. [PubMed: 16928810]
38. Law B, Weissleder R, Tung C-H. Peptide-based biomaterials for protease-enhanced drug delivery. Biomacromolecules. 2006; 7:1261–1265. [PubMed: 16602747]
39. Guo R, Li R, Li X, Zhang L, Jiang X, Liu B. Dual-functional alginic acid hybrid nanospheres for cell imaging and drug delivery. Small. 2009; 5:709–717. [PubMed: 19235799]
40. Sajja HK, East MP, Mao H, Wang YA, Nie S, Yang L. Development of multifunctional nanoparticles for targeted drug delivery and noninvasive imaging of therapeutic effect. Curr. Drug Discov. Technol. 2009; 6:43–51. [PubMed: 19275541]

41. Taylor-Pashow KML, Rocca JD, Xie Z, Tran S, Lin W. Post synthetic modifications of iron-carboxylate nanoscale metal-organic frameworks for imaging and drug delivery. J. Am. Chem. Soc. 2009; 131:14261–14263. [PubMed: 19807179]
42. McCarthy JR, Weissleder R. Multifunctional magnetic nanoparticles for targeted imaging and therapy. Adv. Drug Deliv. Rev. 2008; 60:1241–1251. [PubMed: 18508157]
43. Gindy ME, Prud'homme RK. Multifunctional nanoparticles for imaging, delivery and targeting in cancer therapy. Expert Opin. Drug Deliv. 2009; 6:865–878. [PubMed: 19637974]
44. Gilchrist RK, Medal R, Shorey WD, Hanselman RC, Parrott JC, Taylor CB. Selective inductive heating of lymph nodes. Ann. Surg. 1957; 146:596–606. [PubMed: 13470751]
45. Lee H, Lee E, Kim DK, Jang NK, Jeong YY, Jon S. Antibiofouling polymer-coated superparamagnetic iron oxide nanoparticles as potential magnetic resonance contrast agents for *in vivo* cancer imaging. J. Am. Chem. Soc. 2006; 128:7383–7389. [PubMed: 16734494]
46. Tiefenauer LX, Kuhne G, Andres RY. Antibody magnetite nanoparticles-invitro characterization of a potential tumor-specific contrast agent for magnetic resonance imaging. Bioconjug. Chem. 1993; 4:347–352. [PubMed: 8274518]
47. Gupta AK, Gupta M. Synthesis and surface engineering of iron oxide nanoparticles for biomedical applications. Biomaterials. 2005; 26:3995–4021. [PubMed: 15626447]
48. Gupta AK, Gupta M. Cytotoxicity suppression and cellular uptake enhancement of surface modified magnetic nanoparticles. Biomaterials. 2005; 26:1565–1573. [PubMed: 15522758]
49. Gupta AK, Curtis ASG. Surface modified superparamagnetic nanoparticles for drug delivery: Interaction studies with human fibroblasts in culture. J. Mater. Sci.-Mater. Med. 2004; 15:493–496. [PubMed: 15332623]
50. Lopez-Perez JA, Lopez-Quintela MA, Mira J, Rivas J. Preparation of magnetic fluids with particles obtained in microemulsions. IEEE Trans. Magn. 1997; 33:4359–4362.
51. Feltin N, Pileni MP. New technique for synthesizing iron ferrite magnetic nanosized particles. Langmuir. 1997; 13:3927–3933.
52. Rockenberger J, Scher EC, Alivisatos PA. A new nonhydrolytic single-precursor approach to surfactant-capped nanocrystals of transition metal oxides. J. Am. Chem. Soc. 1999; 121:11595–11596.
53. Berry CC, Curtis ASG. Functionalisation of magnetic nanoparticles for applications in biomedicine. J. Phys. D-Appl. Phys. 2003; 36:R198–R206.
54. Berry CC, Wells S, Charles S, Curtis ASG. Dextran and albumin derivatised iron oxide nanoparticles: Influence on fibroblasts *in vitro*. Biomaterials. 2003; 24:4551–4557. [PubMed: 12950997]
55. Zhang Y, Kohler N, Zhang MQ. Surface modification of superparamagnetic magnetite nanoparticles and their intracellular uptake. Biomaterials. 2002; 23:1553–1561. [PubMed: 11922461]
56. D'Souza AJM, Schowen RL, Topp EM. Polyvinylpyrrolidone-drug conjugate: Synthesis and release mechanism. J. Controll. Release. 2004; 94:91–100.
57. Gupta AK, Curtis ASG. Lactoferrin and ceruloplasmin derivatized superparamagnetic iron oxide nanoparticles for targeting cell surface receptors. Biomaterials. 2004; 25:3029–3040. [PubMed: 14967536]
58. Bulte JWM, Zhang SC, van Gelderen P, Herynek V, Jordan EK, Duncan ID, Frank JA. Neurotransplantation of magnetically labeled oligodendrocyte progenitors: Magnetic resonance tracking of cell migration and myelination. Proc. Natl. Acad. Sci. USA. 1999; 96:15256–15261. [PubMed: 10611372]
59. Peng X-H, Qian X, Mao H, Wang AY, Chen Z, Nie S, Shin DM. Targeted magnetic iron oxide nanoparticles for tumor imaging and therapy. Int. J. Nanomed. 2008; 3:311–321.
60. Ibraimi F, Kriz D, Lu M, Hansson LO, Kriz K. Rapid one-step whole blood C-reactive protein magnetic permeability immunoassay with monoclonal antibody conjugated nanoparticles as superparamagnetic labels and enhanced sedimentation. Anal. Bioanal. Chem. 2006; 384:651–657. [PubMed: 16240109]

61. Gruttner C, Muller K, Teller J, Westphal F, Foreman A, Ivkov R. Synthesis and antibody conjugation of magnetic nanoparticles with improved specific power absorption rates for alternating magnetic field cancer therapy. J. Magn. Magn. Mater. 2007; 311:181–186.
62. Josephson L, Tung CH, Moore A, Weissleder R. High-efficiency intracellular magnetic labeling with novel superparamagnetic-tat peptide conjugates. Bioconjug. Chem. 1999; 10:186–191. [PubMed: 10077466]
63. Lewin M, Carlesso N, Tung CH, Tang XW, Cory D, Scadden DT, Weissleder R. Tat peptide-derivatized magnetic nanoparticles allow *in vivo* tracking and recovery of progenitor cells. Nat. Biotechnol. 2000; 18:410–414. [PubMed: 10748521]
64. Faust A, Hermann S, Wagner S, Haufe G, Schober O, Schafers M, Kopka K. Molecular imaging of apoptosis *in vivo* with scintigraphic and optical biomarkers - A status report. Anti-Cancer Agents Med. Chem. 2009; 9:968–985.
65. Wagner K, Kautz A, Roder M, Schwalbe M, Pachmann K, Clement JH, Schnabelrauch M. Synthesis of oligonucleotide-functionalized magnetic nanoparticles and study on their *in vitro* cell uptake. Appl. Organometallic Chem. 2004; 18:514–519.
66. Matsumura Y, Maeda H. A new concept for macromolecular therapeutics in cancer chemotherapy: mechanism of tumoritropic accumulation of proteins and the antitumor agent smancs. Cancer Res. 1986; 46:6387–6392. [PubMed: 2946403]
67. Luk JMC, Lindberg AA. Rapid and sensitive detection of salmonella (0-6, 7) by immunomagnetic monoclonal antibody-based assays. J. Immunol. Methods. 1991; 137:1–8. [PubMed: 1707080]
68. Koh I, Hong R, Weissleder R, Josephson L. Nanoparticle-target interactions parallel antibody-protein interactions. Anal. Chem. 2009; 81:3618–3622. [PubMed: 19323458]
69. Chen J, Tung CH, Allport JR, Chen S, Weissleder R, Huang PL. Near-infrared fluorescent imaging of matrix metalloproteinase activity after myocardial infarction. Circulation. 2005; 111:1800–1805. [PubMed: 15809374]
70. Bremer C, Tung CH, Weissleder R. *In vivo* molecular target assessment of matrix metalloproteinase inhibition. Nat. Med. 2001; 7:743–748. [PubMed: 11385514]
71. Bremer C, Bredow S, Mahmood U, Weissleder R, Tung CH. Optical imaging of matrix metalloproteinase-2 activity in tumors: Feasibility study in a mouse model. Radiology. 2001; 221:523–529. [PubMed: 11687699]
72. Rezaeipoor R, John R, Adie SG, Chaney EJ, Marjanovic MA, Oldenburg AL, Rinne SA, Boppart SA. Fc-directed antibody conjugation of magnetic nanoparticles for enhanced molecular targeting. J. Innovative Opt. Health Sci. 2009; 2:387–396.
73. Josephson L, Kircher MF, Mahmood U, Tang Y, Weissleder R. Near-infrared fluorescent nanoparticles as combined MR/optical imaging probes. Bioconjug. Chem. 2002; 13:554–560. [PubMed: 12009946]
74. Jing Y, Mal N, Williams PS, Mayorga M, Penn MS, Chalmers JJ, Zborowski M. Quantitative intracellular magnetic nanoparticle uptake measured by live cell magnetophoresis. FASEB J. 2008; 22:4239–4247. [PubMed: 18725459]
75. Lee TM, Oldenburg AL, Sitafalwalla S, Marks DL, Luo W, Toublan FJJ, Suslick KS, Boppart SA. Engineered microsphere contrast agents for optical coherence tomography. Opt. Lett. 2003; 28:1546–1548. [PubMed: 12956374]
76. Toublan FJJ, Suslick KS, Boppart SA, Lee TM, Oldenburg AL. Modification of protein microspheres for biomedical applications. Abst. Papers Am. Chem. Soc. 2003; 225:324–POLY.
77. Toublan FJJ, Boppart SA, Suslick KS. Tumor targeting by surface-modified protein microspheres. J. Am. Chem. Soc. 2006; 128:3472–3473. [PubMed: 16536492]
78. McDonald MA, Jankovic L, Shahzad K, Burcher M, Li KCP. Acoustic fingerprints of dye-labeled protein submicrosphere photoacoustic contrast agents. J. Biomed. Opt. 2009; 14:034032. [PubMed: 19566325]
79. Oldenburg AL, Toublan FJJ, Suslick KS, Wei A, Boppart SA. Magnetomotive contrast for *in vivo* optical coherence tomography. Opt. Expr. 2005; 13:6597–6614.
80. Hafeli, U.; Schutt, W.; Teller, J.; Zborowski, M., editors. Scientific and Clinical Applications of Magnetic Carriers. Plenum Press; 1997.

81. Romanus E, Huckel M, Gross C, Prass S, Weitschies W, Brauer R, Weber PJ. Magnetic nanoparticle relaxation measurement as a novel tool for in vivo diagnostics. J. Magn. Magn. Mater. 2002; 252:387–389.
82. Anker JN, Kopelman R. Magnetically modulated optical nanoprobes. Appl. Phys. Lett. 2003; 82:1102–1104.
83. Huang D, Swanson EA, Lin CP, Schuman JS, Stinson WG, Chang W, Hee MR, Flotte T, Gregory K, Puliafito CA, Fujimoto JG. Optical coherence tomography. Science. 1991; 254:1178–1181. [PubMed: 1957169]
84. Swanson EA, Izatt JA, Hee MR, Huang D, Lin CP, Schuman JS, Puliafito CA, Fujimoto JG. *In vivo* retinal imaging by optical coherence tomography. Opt. Lett. 1993; 18:1864–1866. [PubMed: 19829430]
85. Hee MR, Izatt JA, Swanson EA, Huang D, Schuman JS, Lin CP, Puliafito CA, Fujimoto JG. Optical coherence tomography of the human retina. Archiv. Ophthalmol. 1995; 113:325–332.
86. Morgner U, Drexler W, Kartner FX, Li XD, Pitris C, Ippen EP, Fujimoto JG. Spectroscopic optical coherence tomography. Opt. Lett. 2000; 25:111–113. [PubMed: 18059799]
87. Boppart SA, Bouma BE, Pitris C, Southern JF, Brezinski ME, Fujimoto JG. *In vivo* cellular optical coherence tomography imaging. Nat. Med. 1998; 4:861–865. [PubMed: 9662382]
88. Boppart SA, Bouma BE, Pitris C, Brezinski ME, Fujimoto JG. Optical coherence tomography of *in vivo* developmental cellular dynamics. FASEB J. 1998; 12:283.
89. Drexler W, Morgner U, Kartner FX, Pitris C, Boppart SA, Li XD, Ippen EP, Fujimoto JG. *In vivo* ultrahigh-resolution optical coherence tomography. Opt. Lett. 1999; 24:1221–1223. [PubMed: 18073990]
90. Boppart SA. Optical coherence tomography: Technology and applications for neuroimaging. Psychophysiology. 2003; 40:529–541. [PubMed: 14570161]
91. Boppart SA. Optical coherence tomography - Principles applications and advances. Minerva Biotecnol. 2004; 16:211–237.
92. Oldenburg AL, Gunther JR, Boppart SA. Imaging magnetically labeled cells with magnetomotive optical coherence tomography. Opt. Lett. 2005; 30:747–749. [PubMed: 15832926]
93. Boppart SA, Oldenburg AL, Xu CY, Marks DL. Optical probes and techniques for molecular contrast enhancement in coherence imaging. J. Biomed. Opt. 2005; 10:041208.
94. Choma MA, Ellerbee AK, Yang C, Creazzo TL, Izatt JA. Spectral-domain phase microscopy. Opt. Lett. 2005; 30:1162–1164. [PubMed: 15945141]
95. Oh J, Feldman MD, Kim J, Kang HW, Sanghi P, Milner TE. Magneto-motive detection of tissue-based macrophages by differential phase optical coherence tomography. Lasers Surg. Med. 2007; 39:266–272. [PubMed: 17295337]
96. Oldenburg AL, Crecea V, Rinne SA, Boppart SA. Phase-resolved magnetomotive OCT for imaging nanomolar concentrations of magnetic nanoparticles in tissues. Opt. Expr. 2008; 16:11525–11539.
97. John R, Chaney EJ, Boppart SA. Dynamics of magnetic nanoparticle-based contrast agents in tissues tracked using magnetomotive optical coherence tomography. IEEE J. Select. Top. Quantum Electron. 2010; 16:691–697.
98. John R, Rezaeipoor R, Adie SG, Chaney EJ, Oldenburg AL, Marjanovic M, Haldar JP, Sutton B, Boppart SA. *In vivo* magnetomotive optical molecular imaging using targeted magnetic nanoprobes. Proc. Natl. Acad. Sci. USA. 2010; 107:8085–8090. [PubMed: 20404194]
99. Camp RL, Dolled-Filhar M, Bonnie LK, Rimm DL. Quantitative analysis of breast cancer tissue microarrays shows that both high and normal levels of *HER2* expression are associated with poor outcome. Cancer Res. 2003; 63:1445–1448. [PubMed: 12670887]
100. Crecea V, Oldenburg AL, Liang X, Ralston TS, Boppart SA. Magnetomotive nanoparticle transducers for optical rheology of viscoelastic materials. Opt. Expr. 2009; 17:23114–23122.
101. Oldenburg AL, Boppart SA. Resonant acoustic spectroscopy of soft tissues using embedded magnetomotive nanotransducers and optical coherence tomography. Phys. Med. Biol. 2010; 55:1189–1201. [PubMed: 20124653]
102. Kim J, Oh J, Milner TE, Nelson JS. Hemoglobin contrast in magnetomotive optical Doppler tomography. Opt. Lett. 2006; 31:778–780. [PubMed: 16544621]

103. Kim J, Oh J, Milner TE, Nelson JS. Imaging nanoparticle flow using magneto-motive optical Doppler tomography. Nanotechnology. 2007; 18:035504. [PubMed: 19636123]
104. Barton J, Stromski S. Flow measurement without phase information in optical coherence tomography images. Opt. Expr. 2005; 13:5234–5239.
105. Mariampillai A, Standish BA, Moriyama EH, Khurana M, Munce NR, Leung MKK, Jiang J, Cable A, Wilson BC, Vitkin IA, Yang VXD. Speckle variance detection of microvascular using swept-source optical coherence tomography. Opt. Lett. 2008; 33:1530–1532. [PubMed: 18594688]
106. Mariampillai A, Leung MKK, Jarvi M, Standish BA, Lee K, Wilson BC, Vitkin A, Yang VXD. Optimized speckle variance OCT imaging of microvasculature. Opt. Lett. 2010; 35:1257–1259. [PubMed: 20410985]
107. Kim J, Oh J, Choi B. Magnetomotive laser speckle imaging. J. Biomed. Opt. 2010; 151:011110. [PubMed: 20210436]
108. Oh J, Feldman MD, Kim J, Condit C, Emelianov S, Milner TE. Detection of magnetic nanoparticles in tissue using magneto-motive ultrasound. Nanotechnology. 2006; 17:4183–4190. [PubMed: 21727557]
109. Mehrmohammadi M, Oh J, Ma L, Yantsen E, Larson T, Mallidi S, Park S, Johnston KP, Sokolov K, Milner T, Emelianov S. Imaging of iron oxide nanoparticles using magneto-motive ultrasound. IEEE Ultrasonics Symposium. 2007:652–655.
110. Ji XJ, Shao RP, Elliott AM, Stafford RJ, Esparza-Coss E, Bankson JA, Liang G, Luo ZP, Park K, Markert JT, Li C. Bifunctional gold nanoshells with a superparamagnetic iron oxide-silica core suitable for both MR imaging and photothermal therapy. J. Phys. Chem. C. 2007; 111:6245–6251.
111. Lu QH, Yao KL, Xi D, Liu ZL, Luo XP, Ning Q. Synthesis and characterization of composite nanoparticles comprised of gold shell and magnetic core/cores. J. Magn. Magn. Mater. 2006; 301:44–49.
112. Kotitz R, Fannin PC, Trahms L. Time-domain study of brownian and neel relaxation in ferrofluids. J. Magn. Magn. Mater. 1995; 149:42–46.
113. Pakhomov AB, Bao YP, Krishnan KM. Effects of surfactant friction on Brownian magnetic relaxation in nanoparticle ferrofluids. J. Appl. Phys. 2005; 97:10Q305/1–10Q305/3.
114. Oleson JR, Calderwood SK, Coughlin CT, Dewhirst MW, Gerweck LE, Gibbs FA, Kapp DS. Biological and clinical aspects of hyperthermia in cancer therapy. J. Clin. Oncol. 1988; 11:368–380.
115. Perez, CA.; Emami, B.; Myerson, RJ. Hyperthermia: In Principle and Practice of Radiation Oncology. Lippincott; Philadelphia: 1992.
116. Johannsen M, Thiesen B, Jordan A, Taymoorian K, Gneveckow U, Waldofner N, Scholz R, Koch M, Lein M, Jung K, Loening SA. Magnetic fluid hyperthermia (MFH) reduces prostate cancer growth in the orthotopic Dunning R3327 rat model. Prostate. 2005; 64:283–292. [PubMed: 15726645]
117. Maier-Hauff K, Rothe R, Scholz R, Gneveckow U, Wust P, Thiesen B, Feussner A, von Deimling A, Waldoefner N, Felix R, Jordan A. Intracranial thermotherapy using magnetic nanoparticles combined with external beam radiotherapy: Results of a feasibility study on patients with glioblastoma multiforme. J. Neuro-Oncol. 2007; 81:53–60.
118. Murray TG, Steeves RA, Gentry L, Bresnick G, Boldt HC, Mieler WF, Tompkins D. Ferromagnetic hyperthermia: functional and histopathologic effects on normal rabbit ocular tissue. Int. J. Hyperthermia. 1997; 13:423–436. [PubMed: 9278771]
119. Jordan A, Scholz R, Wust P, Fahling H, Krause J, Wlodarczyk W, Sander B, Vogl T, Felix R. Effects of magnetic fluid hyperthermia (MFH) on C3H mammary carcinoma *in vivo*. Int. J. Hyperthermia. 1997; 13:587–605. [PubMed: 9421741]
120. Kenneth D, Charles S, Kevin L, Guoda L, Donald G, Matthew J. Epithelial internalization of superparamagnetic nanoparticles and response to external magnetic field. Biomaterials. 2005; 26:2061–2072. [PubMed: 15576180]

121. Hilger I, Andra W, Hergt R, Hiergeist R, Schubert H, Kaiser WA. Electromagnetic heating of breast tumors in interventional radiology: *In vitro* and *in vivo* studies in human cadavers and mice. Radiology. 2001; 218:570–575. [PubMed: 11161180]

122. Drake P, Cho H-J, Shih P-S, Kao C-H, Lee K-F, Kuo C-H, Lin X-Z, Lin Y-J. Gd-doped iron-oxide nanoparticles for tumour therapy via magnetic field hyperthermia. J. Mater. Chem. 2007; 17:4914–4918.

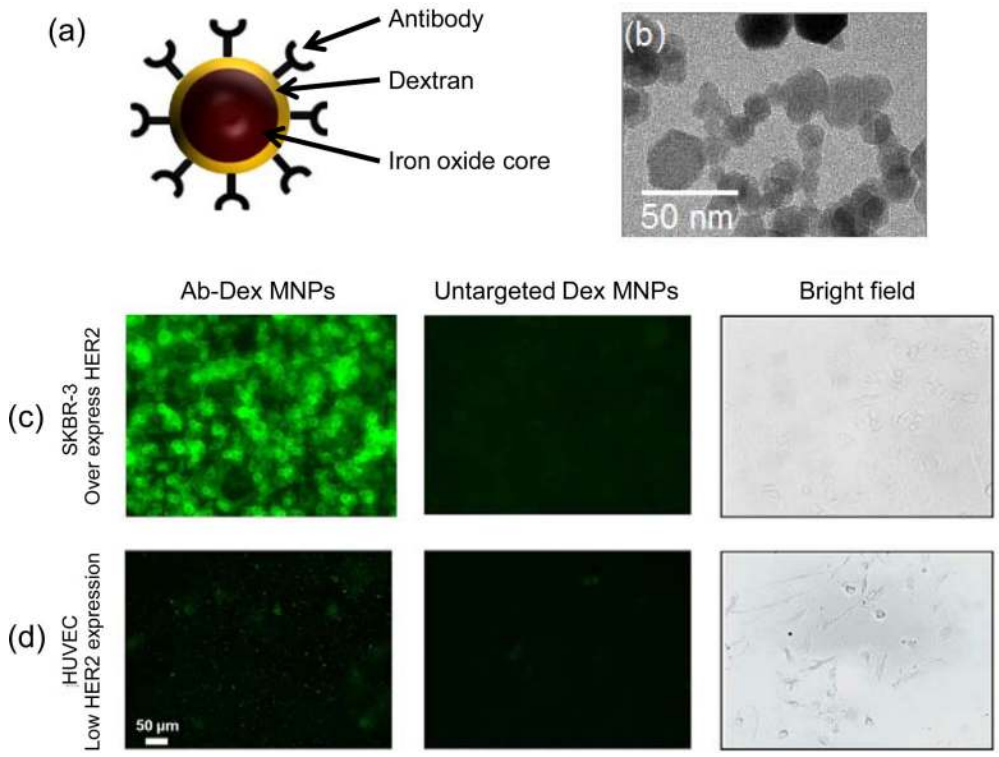

Fig. (1).

Molecular imaging using dextran-coated iron oxide nanoparticles functionalized with anti-*HER2* antibody. (**a**) Schematic representation. (**b**) TEM. (c,d) Fluorescent and brightfield microscope images showing *HER2* targeting using functionalized nanoparticles on SKBR-3 cells that over-express *HER2* and HUVEC cells that have low expression of *HER2*. Images in (**c**,**d**) were reproduced with permission from [72]. Copyright, World Scientific Publishing Co. Pte. Ltd. (For interpretation of the references to color in this figure legend, the reader is referred to the web version of this paper).

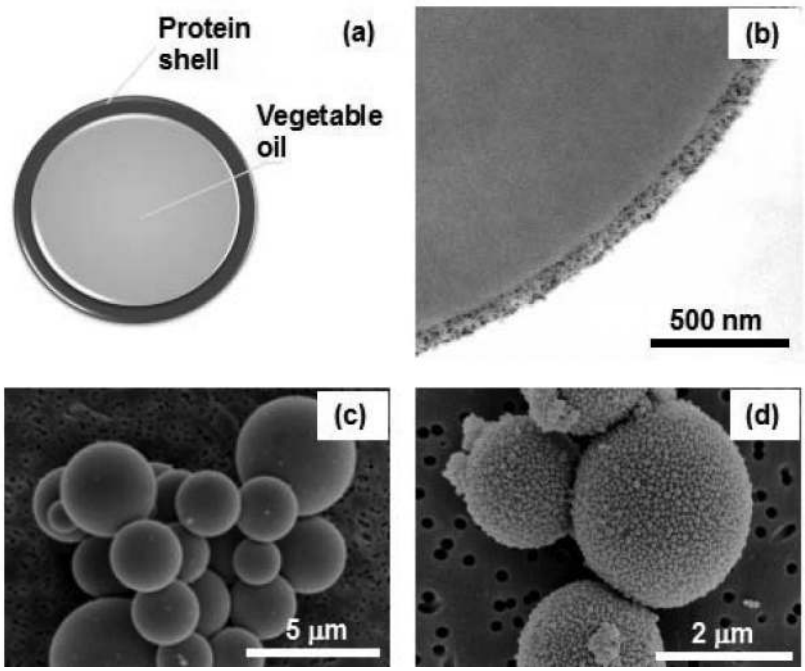

Fig. (2).
Protein microspheres as multifunctional multimodal contrast agents with flexible fabrication parameters allowing modifications of surface, shell and core contents. (**a**) Schematic representation of oil-filled protein microsphere. (**b**) TEM showing magnified view of the shell. (**c**) SEM of non-conjugated protein microspheres. (**d**) SEM of RGD poly-lysine peptide conjugated protein microspheres.

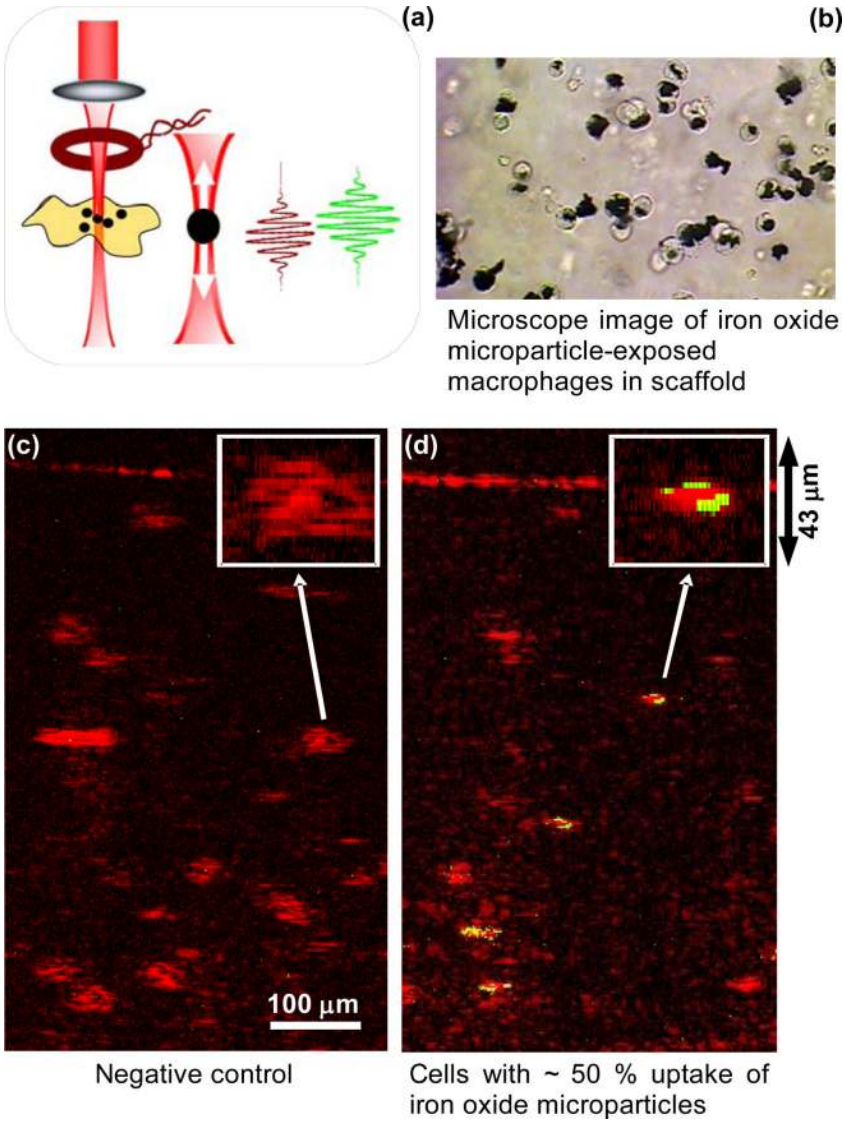

Fig. (3).

(**a**) Magnetomotion principle. Representative images of macrophage cells in three-dimensional scaffolds are shown by (**b**) light microscopy and (**c**, **d**) structural OCT (red) and MM-OCT (green) signals. Control macrophages and macrophages allowed to uptake magnetite microparticles are shown in (**c**) and (**d**), respectively. Apparent cell sizes (approximately 8–30 μm) are consistent with light microscopy observations. (**c-d**) images reproduced with permission from [92]. Copyright, Optical Society of America, 2005. (For interpretation of the references to color in this figure legend, the reader is referred to the web version of this paper).

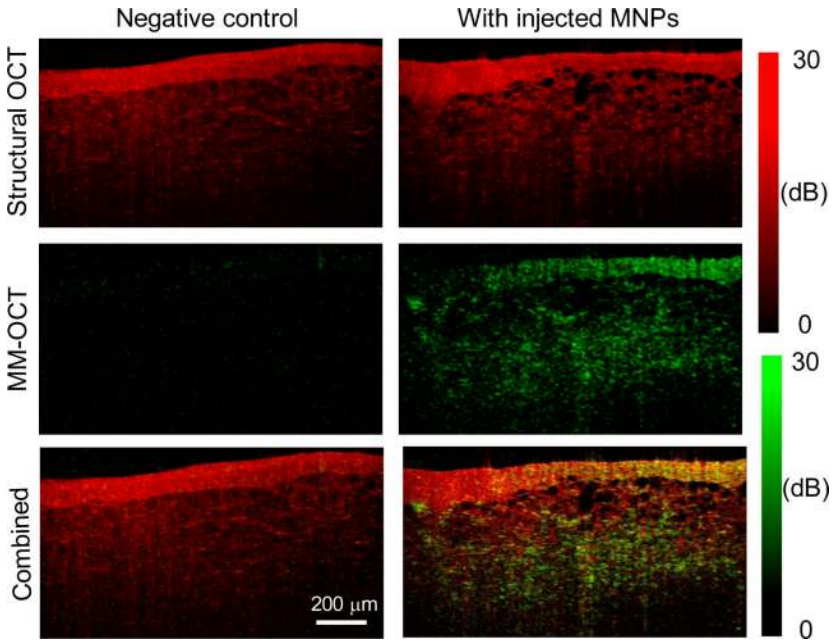

Fig. (4).
MM-OCT in tissue. Images were acquired from *in vitro* chicken breast tissue. Structural and MM-OCT images were acquired in tandem, without and with the administration of iron-oxide nanoparticles. Figure reprinted with permission [93]. Copyright, SPIE, 2005. (For interpretation of the references to color in this figure legend, the reader is referred to the web version of this paper).

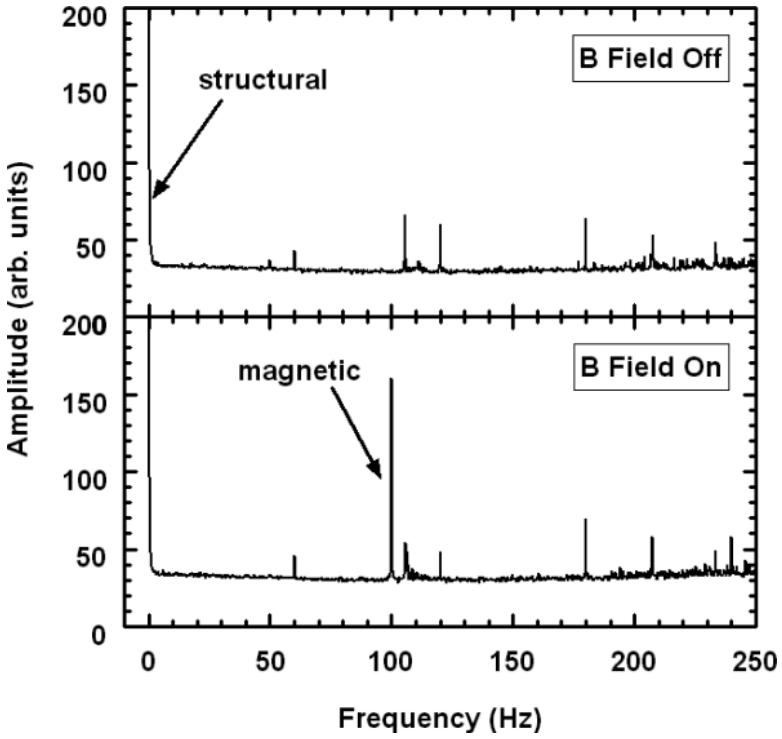

Fig. (5).

Representative transverse Fourier spectra with and without magnetic field modulation at 100 Hz for B-mode imaging of a tissue phantom with 100 μg/g of MNPs. Spectral amplitudes were averaged over all rows of the image. As indicated, the low frequency peak contains the usual structural OCT data, and a peak at 100 Hz is specific to magnetomotion. Other peaks are attributed to background noise (including 60 Hz and its harmonics). Figure reproduced with permission from [96]. Copyright, Optical Society of America, 2008.

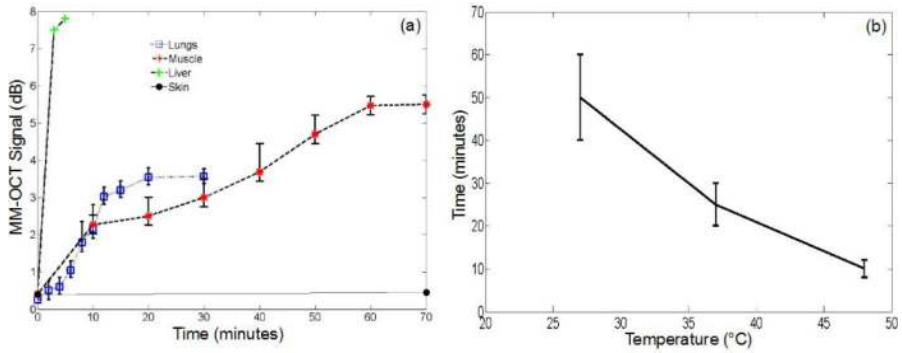

Fig. (6).

(**a**) Results showing MM-OCT signal intensity corresponding to transport of MNPs in different tissue types as a function of time. (**b**) Time versus temperature plot for MNP transport through muscle tissue. The vertical axis denotes the time taken for obtaining a saturated MM-OCT signal and horizontal axis shows the temperature in °C. Figures reproduced with permission from [97]. Copyright, IEEE Photonics Society, 2010. (For interpretation of the references to color in this figure legend, the reader is referred to the web version of this paper).

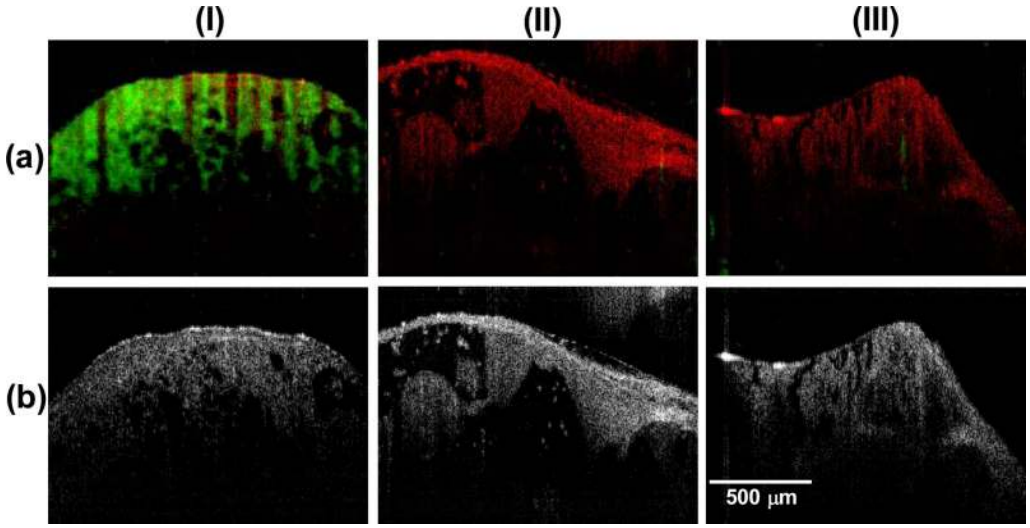

Fig. (7).
In vivo MM-OCT imaging of anti *HER2* antibody functionalized MNPs in a preclinical mammary tumor model. (**a**) MM-OCT and (**b**) OCT images from (I) targeted MNP-injected, (II) non-targeted MNP-injected, and (III) saline-injected rats. MM-OCT signal (green channel) is superposed on the OCT signal (red channel). Figure reproduced with permission from [98]. Copyright, National Academy of Sciences, 2010. (For interpretation of the references to color in this figure legend, the reader is referred to the web version of this paper).

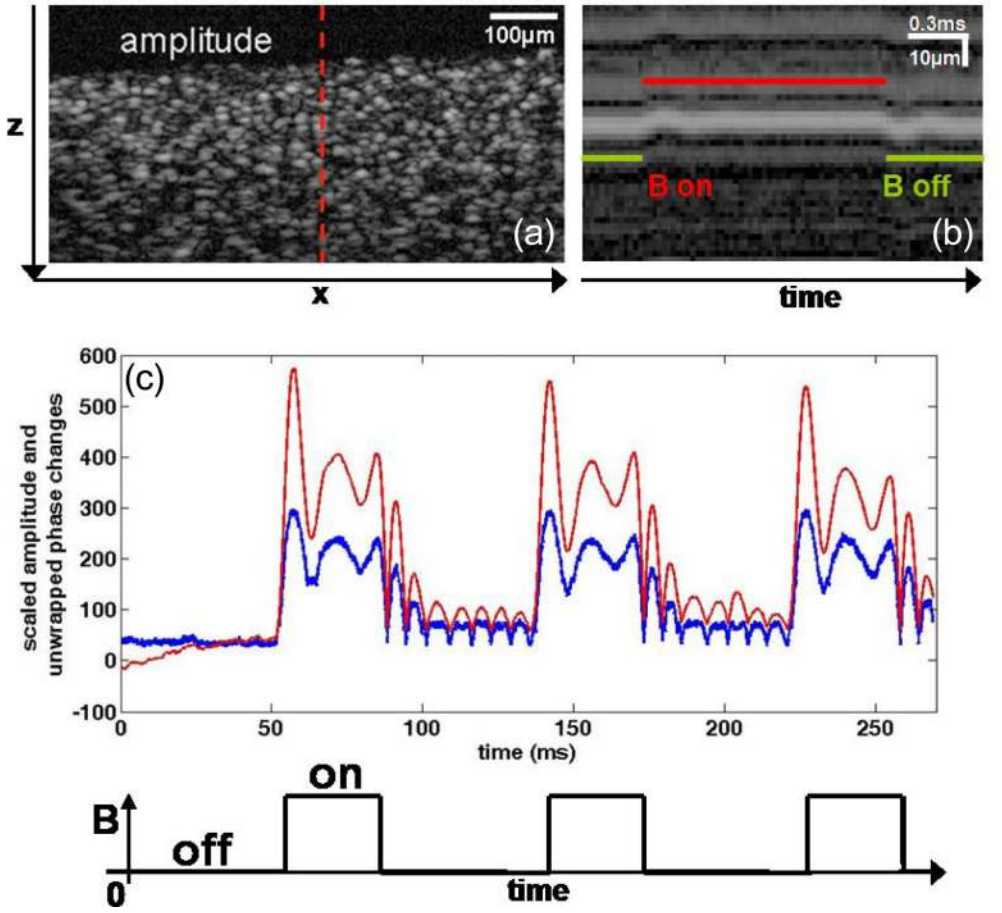

Fig. (8).

Scatterer response upon step-wise modulation of a magnetic field. (**a**) Two-dimensional (x-z) cross-sectional (B-mode) amplitude OCT image of a silicone sample containing MNPs and TiO_2 optical scatterers. The dashed line indicates the location in sample where M-mode imaging is performed with MMOCE. (**b**) M-mode amplitude OCT image of a region of scatterers acquired while the magnetic field is applied step-wise. (**c**) Average time-dependent scatterer changes along one axial position, illustrating both the changes in phase (red) and changes in amplitude (blue) as the magnetic field is applied step-wise, relative to an idle state with zero magnetic field. Figure reproduced with permission from [100]. Copyright, Optical Society of America, 2009. (For interpretation of the references to color in this figure legend, the reader is referred to the web version of this paper).